Article

Aldol Condensation of Acetaldehyde over Titania, Hydroxyapatite and Magnesia

Zachary D Young, Sabra Hanspal, and Robert J Davis

ACS Catal., **Just Accepted Manuscript** • DOI: 10.1021/acscatal.6b00264 • Publication Date (Web): 07 Apr 2016

Aldol Condensation of Acetaldehyde over Titania, Hydroxyapatite and Magnesia

*Zachary D. Young, Sabra Hanspal and Robert J. Davis**

University of Virginia Chemical Engineering Department

102 Engineers' Way

P.O. Box 400741

Charlottesville, VA 22904-4741

*rjd4f@virginia.edu

Abstract

The kinetics of aldol condensation of acetaldehyde were studied over anatase titania (TiO_2), hydroxyapatite (HAP) and magnesia (MgO). Reactions were carried out in a fixed bed reactor with a total system pressure of 220 kPa at temperatures between 533 and 633 K and acetaldehyde partial pressures between 0.05 and 50 kPa. Crotonaldehyde was the only product observed over all three catalysts and severe catalyst deactivation occurred at acetaldehyde partial pressures of 5 kPa or greater. The aldol condensation reaction over all three catalysts was first order at low acetaldehyde partial pressure and approached zero order at high acetaldehyde partial pressure. No kinetic isotope effect (KIE) was observed with fully deuterated acetaldehyde reacting over TiO_2 or HAP implying C-H bond activation is not kinetically relevant. These measurements are consistent with a mechanism in which adsorption and desorption steps are kinetically significant during the reaction. Characterization of the catalysts by adsorption microcalorimetry of acetaldehyde and ethanol and diffuse reflectance Fourier transformed infrared spectroscopy of adsorbed acetaldehyde, crotonaldehyde and acetic acid revealed a very high reactivity of these catalysts, even at low temperatures.

Key Words: Aldol Condensation, Guerbet Coupling, DRIFTS, Microcalorimetry, Kinetic Isotope Effect

1. Introduction

Large quantities of bio-renewable ethanol are produced globally every year for use as a fuel additive with the United States being the largest producer of bio-ethanol. However, ethanol is a relatively poor fuel additive due to its corrosiveness, high miscibility with water, and low energy density. Butanol is considered to be a better fuel additive due to its higher energy density and lower miscibility with water. Unfortunately, butanol is currently produced from fossil fuel sources through the energy intensive hydroformylation process (also known as the oxo process). To use butanol as a biorenewable fuel additive requires producing butanol from a biorenewable source. This can be accomplished by converting bio-ethanol to butanol through the Guerbet coupling reaction.

Guerbet coupling is a sequence of reactions that results in the formation of a long chain saturated alcohol from two shorter chain saturated alcohols. Guerbet coupling is thought to consist of many elementary steps including dehydrogenation, aldol condensation, and hydrogenation. Many heterogeneous catalytic systems have been studied for this reaction including, for example, magnesia (MgO),[1–5] Mg-Al mixed metal oxides[1,6] and hydroxyapatite (HAP).[4,5,7–10] For more information on heterogeneous systems used for Guerbet coupling see the recent review by Kozlowski and Davis.[11]

Although the mechanism of Guerbet coupling of ethanol is still debated, it is generally thought to proceed through the following sequence of steps. First, ethanol is dehydrogenated to acetaldehyde, two molecules of acetaldehyde form crotonaldehyde through aldol condensation and finally crotonaldehyde is hydrogenated to form saturated 1-butanol. The final hydrogenation step likely involves hydrogen transfer from ethanol to regenerate acetaldehyde through a Meerwein-Ponndorf-Verlery like step which has been shown to be very active over

hydroxyapatite.[12] The aldol condensation of acetaldehyde has been proposed to be the rate determining step of this reaction over strontium-substituted hydroxyapatite.[8] Additionally a recent publication by Ho et al. has stated that enolate formation is the rate determining step in Guerbet coupling of ethanol over hydroxyapatite.[13] In contrast, Scalbert et al. use a thermodynamic argument to claim aldol condensation plays only a minor role in butanol formation from ethanol over HAP at temperatures between 633 and 673 K.[14] Chieregato et al. have also questioned the relevance of aldol condensation over MgO stating that Guerbet coupling proceeds through a direct condensation mechanism.[15] In an attempt to elucidate the role of aldol condensation in the Guerbet coupling reaction, the aldol condensation of acetaldehyde was studied over a series of catalysts.

Aldol condensation is a well-studied reaction that forms a carbon-carbon bond between two aldehyde or ketone molecules. Aldol condensation is a critical step in the production of 2-ethyhexanal, isophorone and crotonaldehyde. This reaction can be catalyzed by a wide variety of solid acid or base catalyst such as zeolites,[16] hydrotalcites and hydrotalcite-derived materials,[1,17–21] metal oxides and supported metal oxides[22–29] and hydroxyapatite.[30]

In the current study, rate measurements were carried out over multiple catalysts to explore the kinetic mechanism of aldol condensation and provide insight to the Guerbet coupling of ethanol. The condensation reaction was studied over three catalysts, anatase TiO_2, HAP and MgO. Both HAP and MgO are common Guerbet coupling catalysts whereas TiO_2 is a commonly-studied catalyst for aldol condensation. Diffuse reflectance infrared Fourier transform spectroscopy (DRIFTS) and adsorption microcalorimetry of various probe molecules were used to probe the affinity of catalyst surfaces for species relevant to the condensation reaction.

2. Materials and Methods

2.1 Catalyst Synthesis

A near stoichiometric hydroxyapatite was synthesized using the co-precipitation method described by Tsuchida et al.[7] Briefly, 200 cm^3 of 0.5 M calcium nitrate tetrahydrate ($Ca(NO_3)_2•(H_2O)_4$, Acros Organics) and 200 cm^3 of 0.3 M diammonium phosphate ($(NH_4)_2HPO_4$, Aldrich, >99.99%) adjusted to pH 10 using ammonium hydroxide were added dropwise to 100 cm^3 of distilled and deionized water at 353 K. The slurry was left for 24 h at 353 K while stirring. The resulting powder was filtered and washed with distilled and deionized water 3 times and dried overnight in air at 373 K.

Commercially-available magnesia (Ube Material Industries, Ltd., Lot Number 109071725) and anatase titania (Aldrich, 99.8%) were purchased. All three catalysts were thermally-treated at 873 K under 100 cm^3 min^{-1} flowing air for 2 h prior to characterization and use in reaction. The powders were subsequently pelletized, crushed and sieved to 106-180 μm.

2.2 Catalyst Characterization

X-ray diffraction (XRD) was performed with a PANalytical X'Pert Pro diffractometer using Cu Kα radiation to verify crystal structure and phase purity.

Elemental analysis of HAP was performed by Galbraith Laboratories (Knoxville, TN) using inductively coupled plasma optical emission spectroscopy (ICP-OES) for calcium and phosphorous content.

Catalyst surface area was obtained from N_2 adsorption at 77 K on a Micromeritics ASAP 2020 automated analyzer using the BET method.

2.3 Aldol Condensation of Acetaldehyde

Kinetic studies were carried out in a stainless steel, downward flow, fixed bed reactor. Prior to reaction, HAP and MgO were heated *in situ* at 773 K for 1 h in 100 cm^3 min^{-1} dry air (GTS-

Welco) while TiO_2 was heated for 2 h at 773 K in 100 cm^3 min^{-1} dry air. A dinitrogen (GTS-Welco, 99.999%) stream containing acetaldehyde was passed over the catalyst for 10 min prior to product analysis with an on-line gas chromatograph equipped with a PoraPLOT Q-HT column and flame ionization detector. The concentration of acetaldehyde was controlled by diluting the saturated dinitrogen stream with flowing dinitrogen as well as cooling the saturator with either a water-ice bath or a dry ice-acetone bath. The total system pressure was maintained at 220 kPa using a back pressure regulator.

Aldol condensation in the presence of ethanol was conducted in the same way while flowing ethanol to a vaporizer using a syringe pump. In some cases, ethanol was fed to the catalyst without acetaldehyde to explore Guerbet coupling. The only product alcohol observed during Guerbet coupling was butanol and there were no peaks associated with unknown compounds in the gas chromatograms.

Aldol condensation of fully-deuterated acetaldehyde was carried out using the same reactor described above. The HAP catalyst was pretreated at 773 K for 1 h in 100 cm^3 min^{-1} dinitrogen while TiO_2 was pretreated at 773 K for 2 h in 100 cm^3 min^{-1} dry air for 2 h. There was no observed difference in reactivity over HAP pretreated in dinitrogen versus HAP pretreated in dry air. Unlabeled acetaldehyde reacted over the catalyst until steady state was achieved, and then the feed was quickly switched to fully-deuterated acetaldehyde (Cambridge Isotopes, 99%). After 4 h, the reactant was switched back to unlabeled acetaldehyde.

All nonlinear fits were done using the least squares curve fitting algorithm lsqcurvefit in Matlab.

2.4 Adsorption Microcalorimetry

Adsorption microcalorimetry experiments were performed using a home built heat-flow microcalorimeter described previously.[31–34] A sample was first outgassed at 773 K for 16 h at 10^{-2} Pa. The treated sample was then cooled and placed in an isothermal block maintained at 303 K for 2 h to reach thermal equilibrium. The sample was exposed to doses of acetaldehyde or ethanol via a volumetric dosing system and each dose was allowed to reach equilibrium with the sample over 15 min. The acetaldehyde (Aldrich, 99.5%) and ethanol (Aldrich, anhydrous, > 99.5%) used in these experiments were further degassed by three freeze-pump-thaw cycles prior to adsorption experiments.

2.5 Diffuse Reflectance Infrared Fourier Transformed Spectroscopy (DRIFTS)

Stepwise temperature-programmed desorption of acetaldehyde, crotonaldehyde, and acetic acid was measured using a Bio-Rad (FTS-60A) FTIR spectrometer equipped with a liquid N_2 cooled MCT detector. A 5 wt% catalyst sample (TiO_2, HAP or MgO) diluted with KBr powder was pretreated at 773 K for 1 h under 30 cm^3 min^{-1} flowing He. Background scans were collected at multiple temperatures after waiting for 15 min to allow the catalyst bed to reach thermal equilibrium. After background scans were collected, a 30 cm^3 min^{-1} He stream passed through a saturator at either room temperature (for crotonaldehyde and acetic acid) or dry ice-acetone temperature (for acetaldehyde). The saturated He stream was passed over the catalyst for 15 min at 303 K. The catalyst was purged with pure He for 15 min at 303 K to remove the gas phase and weakly-adsorbed probe molecules. The temperature was then increased in a stepwise manner while continuously flowing He. Scans were collected at each temperature after the system was allowed to purge for 15 min at that temperature.

3. Results and Discussion

3.1 Catalyst Characterization

The BET surface areas of TiO_2, HAP and MgO were found to be 9, 29 and 35 m^2 g^{-1}, respectively. The ICP-OES results for HAP showed a Ca/P ratio of 1.70 which is very close to the stoichiometric value of 1.67. All catalysts were found to be phase pure and had XRD patterns that matched well with reference patterns as shown in the Supporting Information in Figure S1.

3.2 Aldol Condensation Kinetics

Aldol condensation of acetaldehyde at low conversion was performed over anatase TiO_2, HAP and MgO, and the only product observed over all catalysts was crotonaldehyde. Titania and HAP were active at 553 K while MgO had comparable areal rates at 633 K. In all three cases, significant deactivation was observed over the first 6 hours on stream with acetaldehyde partial pressures of 5 kPa or greater. Typical deactivation curves over the three catalysts in 5 kPa of acetaldehyde are shown in Figure 1. Deactivation is commonly observed during aldol condensation of acetaldehyde over heterogeneous catalysts and is most likely the result of high molecular weight compounds formed by sequential reactions of the product aldehyde.[22,25,27,30]

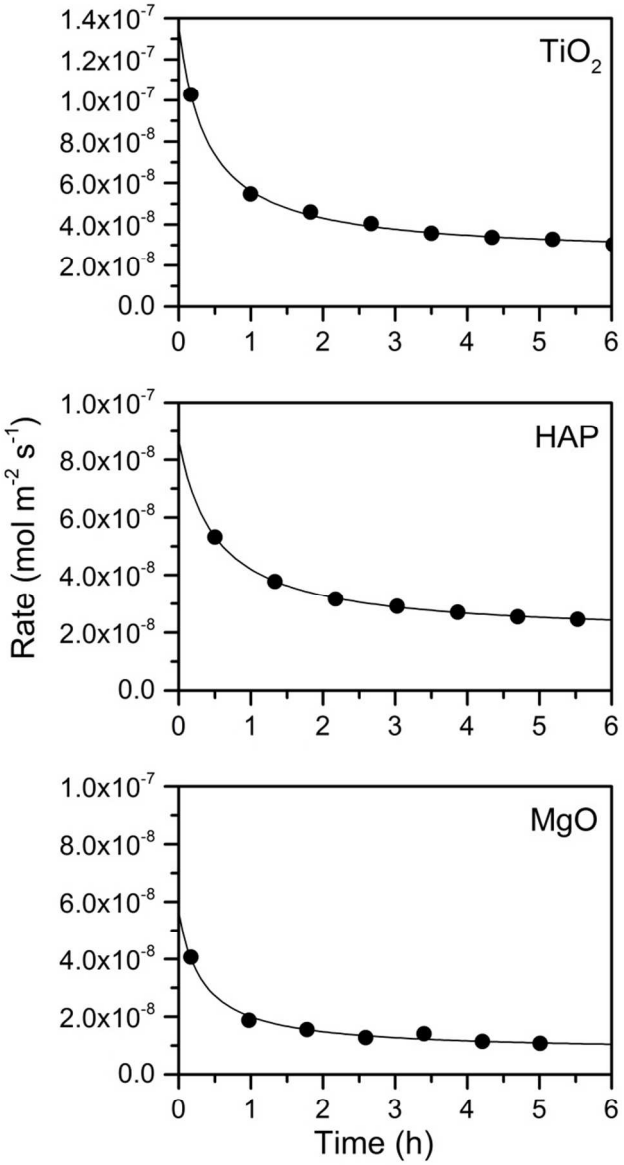

Figure 1. Rates collected over 6 hours at 5 kPa acetaldehyde partial pressure. TiO_2 and HAP were run at 553 K, MgO was run at 673 K. Results were fitted to a three parameter empirical hyperbolic function.

We observed very little deactivation over HAP and TiO_2 at acetaldehyde pressures below 0.4 kPa. In fact, at these low acetaldehyde partial pressures steady state rates were measured over both TiO_2 and HAP. Interestingly, even at very low partial pressures of acetaldehyde, deactivation still occurred over MgO. Figure 2 shows the rate of reaction versus acetaldehyde partial pressure at 553 and 533 K over TiO_2 and HAP under steady state conditions at low acetaldehyde pressure. The order of reaction over HAP at these conditions is 0.9. Interestingly, changing the reaction temperature by 20 K had no measurable effect on the rate of reaction over HAP implying a very low activation energy. The reaction is also first order over TiO_2, but the temperature dependence of the rate indicated an apparent activation energy of 47 kJ mol^{-1}, which is also low. An apparent activation energy for MgO was not measured because of deactivation even at low partial pressures of acetaldehyde.

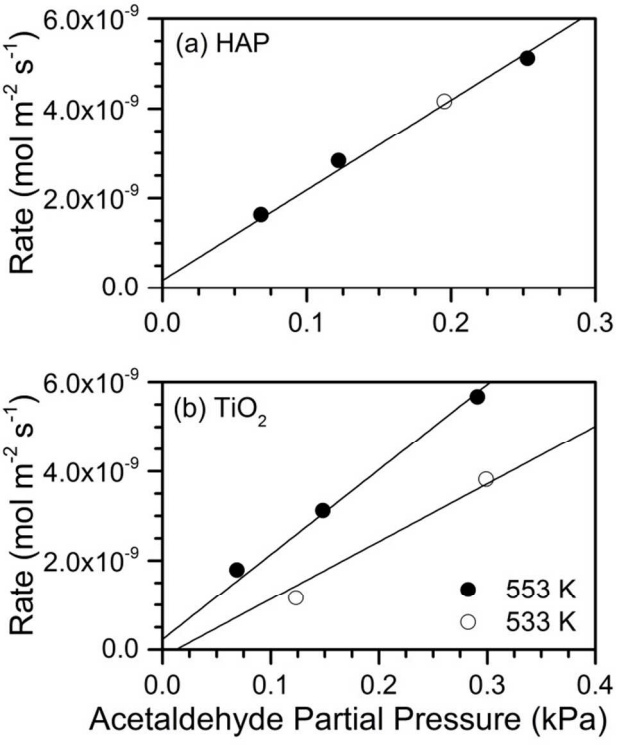

Figure 2. Rate of aldol condensation of acetaldehdye at low partial pressure over (a) HAP and (b) TiO_2.

In an attempt to explore the mechanism of aldol condensation over TiO_2 and HAP, fully deuterated acetaldehyde was used to check for a kinetic isotope effect (KIE). The kinetic isotope studies were carried out at low acetaldehyde partial pressures to avoid the effects of deactivation. Table 1 shows the KIE evaluated over both TiO_2 and HAP. The apparent first order rate constants k_H and k_D were calculated by normalizing the rate of reaction by the acetaldehyde partial pressure. The ratio of k_H to k_D is very close to unity for the reactions on TiO_2 and HAP. The lack of a kinetic isotope effect shows that C-H activation is not kinetically relevant over either catalyst.

Table 1. Kinetic isotope effect for aldol condensation of acetaldehyde over HAP and TiO_2 at 553 K.

Catalyst	**Acetaldehyde Partial Pressure** (kPa)	$\mathbf{k_H}$ (mol kPa^{-1} m^{-2} s^{-1})	$\mathbf{k_D}$ (mol kPa^{-1} m^{-2} s^{-1})	$\boldsymbol{\frac{k_H}{k_D}}$
HAP	0.097	2.5×10^{-8}	2.2×10^{-8}	1.1
TiO_2	0.26	8.6×10^{-9}	8.8×10^{-9}	0.98

Elementary steps for aldol condensation include acetaldehyde adsorption, enolate formation, C-C coupling, dehydration and product desorption. The fact that C-H bond activation is not kinetically relevant implies that enolate formation is not the rate determining step because it is the result of α-H abstraction from the surface-bound aldehyde. Results from adsorption microcalorimetry and infrared spectroscopy, discussed later, indicate that surface reactions of

adsorbed aldehydes occur readily under very mild conditions. If a bimolecular surface reaction between surface enolate and acetaldehyde were rate limiting, the condensation reaction would be second order in acetaldehyde instead of the observed first order. Construction of a Langmuir-Hinshelwood rate equation assuming that desorption of products is rate determining also reveals that the rate would be second order in acetaldehyde at low partial pressures. As described in the Supporting Information, a potential kinetic model that might explain the experimental results involves the irreversible adsorption of acetaldehyde and kinetically relevant desorption of either crotonaldehyde or water as shown in Scheme 1.

Scheme 1

$$AcH + * \xrightarrow{k_1} AcH*$$

$$\cdots$$

$$Product* \xrightarrow{k_2} Product + *$$

In an attempt to further explore the kinetic mechanism, the influence of acetaldehyde on the condensation rate was evaluated at higher partial pressures. Unfortunately, all three catalysts deactivate rapidly at high acetaldehyde partial pressures and steady state rates cannot be measured. Indeed, Rekoske and Barteau discovered severe deactivation of titania during the first 10 minutes of aldol condensation of acetaldehyde under conditions similar to the high pressure acetaldehyde experiments reported here.[27] In an attempt to minimize the influence of deactivation on the reaction kinetics, initial rates were estimated by extrapolating the rate curves over 6 h of reaction to zero time on stream. A three parameter hyperbolic function shown in Equation 1 was used to determine initial rates.

$$r = \frac{c_1}{1 + c_2 t} + c_3 \quad (1)$$

The functional form was found to fit the deactivation curves well as shown in Figure 1. An empirical function such as this is commonly used to model a deactivating catalyst.[35]

The aldol condensation reaction over the three catalysts was performed at multiple acetaldehyde partial pressures and the results are shown in Figure 3. Titania was the most active catalyst (per m^2) for aldol condensation of acetaldehyde followed by HAP and MgO. The activity of MgO was so low that the reaction temperature was increased by 80 K to obtain comparable rates to HAP. All of the catalysts exhibit significant deviation from first order behavior at higher acetaldehyde pressures and some appear to approach zero order. Over TiO_2 the approach to zero order at high acetaldehyde partial pressures is less apparent. Rekoske and Barteau showed that the rate of deactivation is zero order with respect to acetaldehyde partial pressure so the decrease in observed reaction order over titania at higher aldehyde pressure is not the result of a higher rate of deactivation.[27]

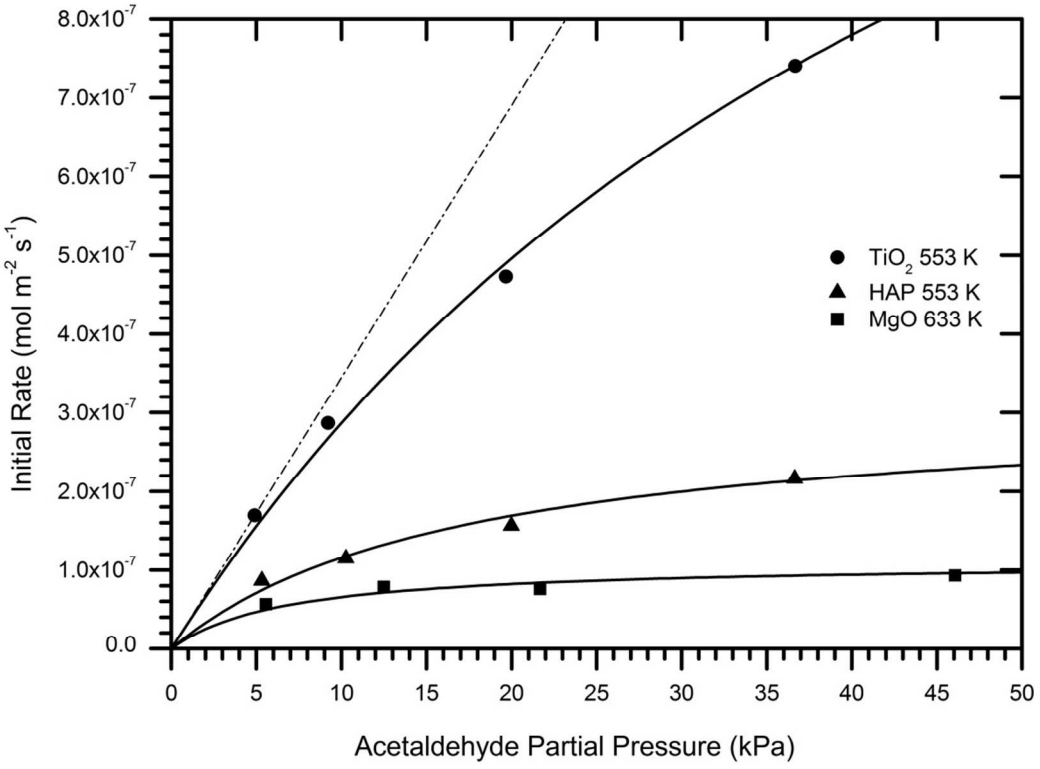

Figure 3. Initial rates of aldol condensation of acetaldehyde over TiO_2, HAP and MgO. The dashed line indicates the expected trend for a first order reaction over TiO_2.

Equation 2 shows the functional form of the rate equation from Scheme 1 as derived in the Supporting Information and assuming that either crotonaldehyde or water is the most abundant surface species

$$r = \frac{\frac{[*]_0 k_1}{2} P_{AcH}}{1 + \frac{k_1}{2k_2} P_{AcH}} \quad (2)$$

where $[*]_0$ is the number density of surface sites, k_1 is the rate constant for acetaldehyde adsorption and k_2 is the rate constant for product desorption.

Equation 2 was used to fit the rates reported in Figure 3. The model parameters were used to extrapolate the high pressure rates to the steady state rates measured at low acetaldehyde partial pressure. The kinetic model was able to predict the observed steady state rates measured at low pressure to within a factor of 2 over TiO_2 and within 30% over HAP. The model agreement involving rates measured at steady state (low pressure) and initial rates measured on a deactivating system (higher pressure) suggests that the initial rates are a reasonable approximation of the steady state rates at higher acetaldehyde partial pressures, although the uncertainty in k_2 could be quite high as it is determined solely by the high pressure initial rates.

The calculated groupings of rate parameters are shown in Table 2. It was not possible to statistically evaluate individual rate constants based on the current data set because the value of $[*]_0$ was highly correlated to k_1. Therefore we need to seek an independent estimate of $[*]_0$, which will be discussed later. The acetaldehyde adsorption rate constant k_1 appears to be relatively similar among the three catalysts, assuming the active site density $[*]_0$ among the catalysts is not too different. The order of magnitude difference in $k_1/2k_2$ suggests the main difference among the catalysts is the rate at which product desorbs from the catalyst surface. Indeed, the fitted values indicate the lowest value of k_2, the product desorption rate constant, is associated with MgO, which is a strong base catalyst, and the greatest value of k_2 is associated with TiO_2. Because the product desorption rate constant has significant uncertainty as it was estimated from rapidly deactivating catalysts, additional information about the interactions of aldehydes with the catalysts is needed to validate the reactivity trends. Hence, we used adsorption microcalorimetry and DRIFTS of adsorbed aldehydes to complement the results derived from reaction kinetics, as will be discussed later.

Table 2. Calculated rate parameters from kinetic model in Equation 2.

Catalyst	T (K)	$[*]_0 k_1/2$ (mol kPa^{-1} m^{-2} s^{-1})	$k_1/2k_2$ (kPa^{-1})
TiO_2	553	3.6 x 10^{-8}	0.021
HAP	553	1.9 x 10^{-8}	0.063
MgO	633	2.6 x 10^{-8}	0.26

At first glance, our results may seem inconsistent with those of Ho et al. who propose enolate formation from acetaldehyde as the rate determining step during Guerbet coupling of ethanol over HAP.[13] Under the conditions of Guerbet coupling, however, ethanol acts as a hydrogen source, resulting in the rapid hydrogenation of crotonaldehyde to butanol. This rapid hydrogen transfer could shift the kinetically-relevant step from product desorption to enolate formation under Guerbet coupling conditions whereas enolate formation appears to be relatively fast under the aldol condensation conditions studied here.

3.3 Aldol Condensation in the Presence of Ethanol

The effect of ethanol partial pressure on acetaldehyde condensation over TiO_2 is shown in Figure S2. Unlike HAP and MgO, TiO_2 did not deactivate in the presence of ethanol. Additionally, the rate of aldol condensation over TiO_2 was inhibited by adding ethanol to the feed. Using the kinetic parameters in Table 2, a competitive adsorption model, shown in Equation 3, was fit to the results. The ethanol co-feeding experiments were performed with 5 kPa acetaldehyde because we did not have the ability to measure accurate product compositions at very low acetaldehyde pressures if ethanol inhibited the aldol condensation rate.

$$r = \frac{\frac{[*]_0 k_1}{2} P_{AcH}}{1 + \frac{k_1}{2k_2} P_{AcH} + K_{EtOH} P_{EtOH}} \quad (3)$$

As seen in Figure 4 this model fits the results well and yields an adsorption equilibrium constant of ethanol K_{EtOH} of 1.3 kPa^{-1} at 553 K under reaction conditions.

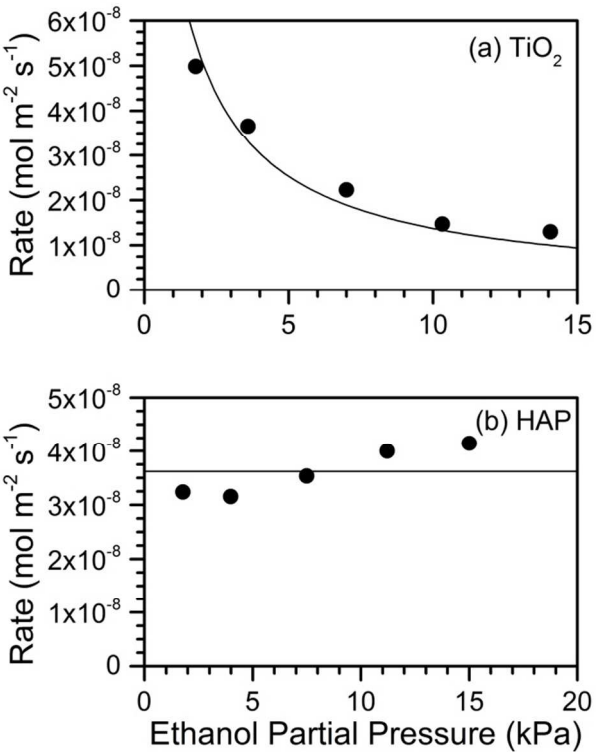

Figure 4. Rate of aldol condensation of acetaldehyde in the presence of ethanol over (a) TiO_2 and (b) HAP. The curve in (a) is a fit to a competitive adsorption model while the line in (b) is the average rate. Reaction conditions: 5 kPa acetaldehyde partial pressure, 553 K.

Ethanol and acetaldehyde were also reacted over HAP at 553 K to compare with results on TiO_2. At this temperature ethanol does not react catalytically on the HAP surface. The effect of added ethanol on the rate of aldol condensation is shown in Figure 4. Over HAP, the added ethanol had little effect of the rate of aldol condensation and the small changes that were observed were the result of slight changes in the deactivation of the catalyst. The time plot of the rate of reaction is shown in Figure S3, which clearly shows that step changes in ethanol partial pressure had no influence on the rate of aldol condensation over HAP.

Cofeeding ethanol and acetaldehyde was also studied over MgO at 633 K. At this temperature, the only product observed during ethanol conversion (no acetaldehyde co-fed) on MgO was a small amount of ethene. The effect of cofeeding ethanol on the acetaldehyde condensation rate over MgO is shown in Figure S4. Step changes in ethanol partial pressure did not result in step changes in the rate of aldol condensation. Although the catalyst continued to deactivate throughout the experiment, there was no evidence that adding ethanol perturbed the aldol condensation rate.

Although the ethanol co-feeding experiments were performed under conditions at which some deactivation was observed, the overall trends in the results are consistent with those derived by aldol condensation reaction kinetics. Specifically, the TiO_2 catalyst appeared to be most affected by the presence of ethanol in the feed indicating a role of competitive adsorption of the alcohol during aldol condensation. Since there did not appear to be any influence of ethanol on the aldol condensation reaction over HAP or MgO, the number density of strongly-bound reaction intermediates and products on those catalysts does not appear to be perturbed by the ethanol. Thus, the combination of reaction kinetics and ethanol co-feeding experiments both point to the conclusion that aldehydes interact strongly with MgO followed by HAP and TiO_2.

3.4 Ethanol conversion

Ethanol conversion was performed over all three catalysts to further investigate the role of aldol condensation on Guerbet coupling. The temperatures of the ethanol reactions were higher than those used to co-feed ethanol so that some catalytic activity could be observed. Table 3 shows the rate of ethanol consumption and the product selectivity over TiO_2, HAP and MgO. At the low levels of conversion during Guerbet coupling of ethanol, the concentration of

acetaldehyde was always below 1 kPa, which is in the low pressure region of the aldol condensation reaction (see Figure 3).

Table 3. Ethanol Reaction (~8 kPa) over HAP, MgO and TiO_2. Results for HAP and MgO were previously reported by Hanspal et al.[5]

Catalyst	T (K)	Conversion (Carbon %)	Rate (mol m^{-2} s^{-1})	Selectivity (C%)				
				Ethene	Ethane	AcH[(a)]	Butanol	Diethyl Ether
TiO_2	613	1.9	1.3×10^{-8}	0	7	51	0	42
HAP	613	4.3	4.4×10^{-8}	1	0	32	67	0
MgO	653	4.5	1.4×10^{-8}	12	0	67	21	0

(a) AcH represents acetaldehyde

Although TiO_2 is the most active catalyst for aldol condensation at lower temperature, it is unable to convert ethanol to butanol at 613 K, instead favoring diethyl ether formation. Since the production of diethyl ether is typically associated with an acidic catalyst, the TiO_2 surface is apparently too acidic to convert ethanol to butanol at elevated temperatures.

The HAP sample is the most active of the three catalysts for Guerbet coupling with a selectivity to butanol of 67% at a temperature 40 K lower than used for MgO.

Magnesia is the least active catalyst, requiring a temperature 40 K higher than HAP and TiO_2 to achieve a similar rate of conversion. Hydroxyapatite has a higher selectivity to butanol while MgO has a higher selectivity to acetaldehyde. The high selectivity towards butanol over HAP is likely due to a large number of appropriate strength acid-base pairs on the surface, which will be discussed in the next section.

3.5 Adsorption Microcalorimetry

Adsorption microcalorimetry was used to investigate the affinity of the catalysts for acetaldehyde and ethanol at 303 K and to estimate an upper bound on the total number of active sites on each catalyst. The acetaldehyde adsorption isotherms and differential heats of adsorption

are shown in Figure 5. A high heat of adsorption as well as a high acetaldehyde uptake were observed on both HAP and MgO. We suspect that a surface reaction occurred during the adsorption microcalorimetry experiment, resulting in higher heats of adsorption and perhaps higher surface coverages than would be expected from simple chemisorption. On TiO_2, the $-\Delta H_{ads}$ of acetaldehyde was much lower compared to that on HAP and MgO. Extrapolating the high pressure linear section of the adsorption isotherm on TiO_2 to zero pressure gives an amount of chemisorbed acetaldehyde of 3.2 μmol m^{-2}, which is in good agreement with the value of 3.7 μmol m^{-2} reported by Rekoske and Barteau.[27] In an analogous fashion, the uptake of acetaldehyde on HAP and MgO was calculated to be 10 and 8.7 μmol m^{-2} respectively, as summarized in Table 4. The lowest values of $-\Delta H_{ads}$ of acetaldehyde were associated with TiO_2, which is completely consistent with the predicted trend in the strength of aldehyde interactions with the catalysts from the reaction kinetics (TiO_2 < HAP < MgO) as discussed earlier.

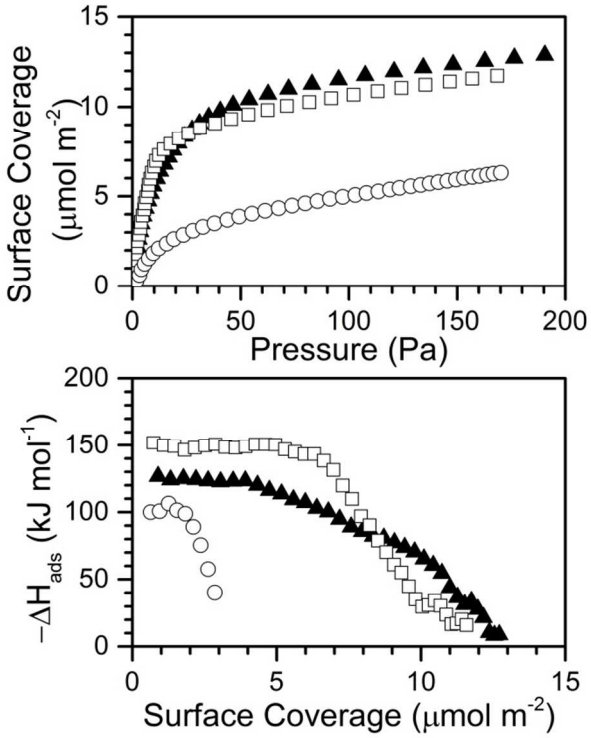

Figure 5. Acetaldehyde uptake (top) and differential heat of adsorption (bottom) over TiO_2 (○), HAP (▲) and MgO (□) at 303 K.

Ethanol adsorption microcalorimetry was also performed over all three catalysts at 303 K. Figure 6 shows the coverage of ethanol and heat of adsorption on TiO_2, HAP and MgO. Extrapolating the high pressure linear portion of the adsorption isotherm to zero pressure gives a coverage of 4.5, 5.2 and 5.2 μmol m^{-2} over TiO_2, HAP and MgO, respectively. The average $-\Delta H_{ads}$ of ethanol on MgO is approximately 118 kJ mol^{-1} while that on both HAP and TiO_2 is approximately 90 kJ mol^{-1}.

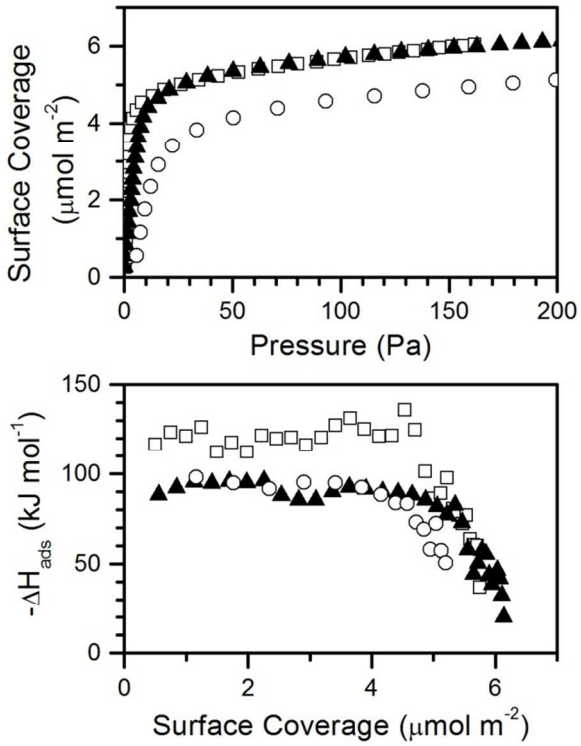

Figure 6. Ethanol uptake (top) and differential heat of adsorption (bottom) over TiO_2 (○), HAP (▲) and MgO (□)at 303 K. Results for MgO were previously reported by Hanspal et al.[5]

The adsorption microcalorimetry results help explain the effect of added ethanol on the rate of acetaldehyde condensation. Hydroxyapatite clearly has a higher affinity for acetaldehyde than TiO_2 whereas both catalysts have a similar affinity for ethanol. The adsorption properties of acetaldehyde are likely similar to those of crotonaldehyde because both molecules have an aldehyde functional group that will interact with the acid-base sites on the surface. The higher affinity of HAP for the aldehyde suggests that under steady state reaction of acetaldehyde, the surface coverage of crotonaldehyde prevents the competitive adsorption of ethanol. The weak affinity of TiO_2 for aldehyde allows the surface to turn over more rapidly, but also allows ethanol to compete for active sites.

We can use the acetaldehyde uptakes reported in Table 4 as an upper bound on the active site density ($[*]_0$) for acetaldehyde condensation on the catalysts. From the results reported in Table 2 and the acetaldehyde uptakes from adsorption microcalorimetry, the individual rate constants for acetaldehyde adsorption (k_1) and product desorption (k_2) were determined and they are summarized in Table 4. Although the rate constant of acetaldehyde adsorption varied by less than a factor of 6 (which may be a function of the assumption of active site density estimate), the rate constant for desorption varied by a factor of almost 50. The rate constant for product desorption is greatest for TiO_2 followed by that for HAP and MgO, which correlates well to the rate of aldol condensation and supports the hypothesis that product desorption is kinetically relevant. We again state here that the numerical value of k_2 was determined from a rapidly deactivating system, so we are drawing conclusions only from the trend in k_2 among the catalysts as opposed to the absolute value of k_2 as a true desorption rate constant.

Table 4. Calculated rate constants for adsorption of acetaldehyde (k_1) and desorption of product (k_2) assuming an active site density based on the uptake of acetaldehyde from adsorption microcalorimetry.

Catalyst	**Acetaldehyde Uptake** (μmol m^{-2})	**Reaction T** (K)	**k_1** (kPa^{-1} s^{-1})	**k_2** (s^{-1})
TiO_2	3.2	553	2.2×10^{-2}	5.3×10^{-1}
HAP	10	553	3.7×10^{-3}	2.9×10^{-2}
MgO	8.7	633	5.9×10^{-3}	1.1×10^{-2}

3.6 DRIFTS

In addition to adsorption microcalorimetry, the catalysts were interrogated by DRIFTS of the adsorbed probe molecules acetaldehyde, crotonaldehyde and acetic acid. Figure 7 shows the carbonyl stretching region of the three probe molecules adsorbed and purged at various temperatures on TiO_2. Adsorbed acetaldehyde had five major features on TiO_2. Peaks at 1708, 1373 and 1288 cm^{-1} were present up to 373 K while peaks at 1575 and 1416 cm^{-1} were observed up to a temperature of 473 K. Adsorbed crotonaldehyde had features at 1722, 1684 and 1622 cm^{-1}, which decreased in intensity as the temperature increased to 573 K. Acetic acid had features at 1724, 1595, 1423 and 1294 cm^{-1}. The peaks at 1724 and 1294 cm^{-1} were not observed at temperatures above 373 K while the peaks at 1595 and 1423 cm^{-1} were observed up to 573 K.

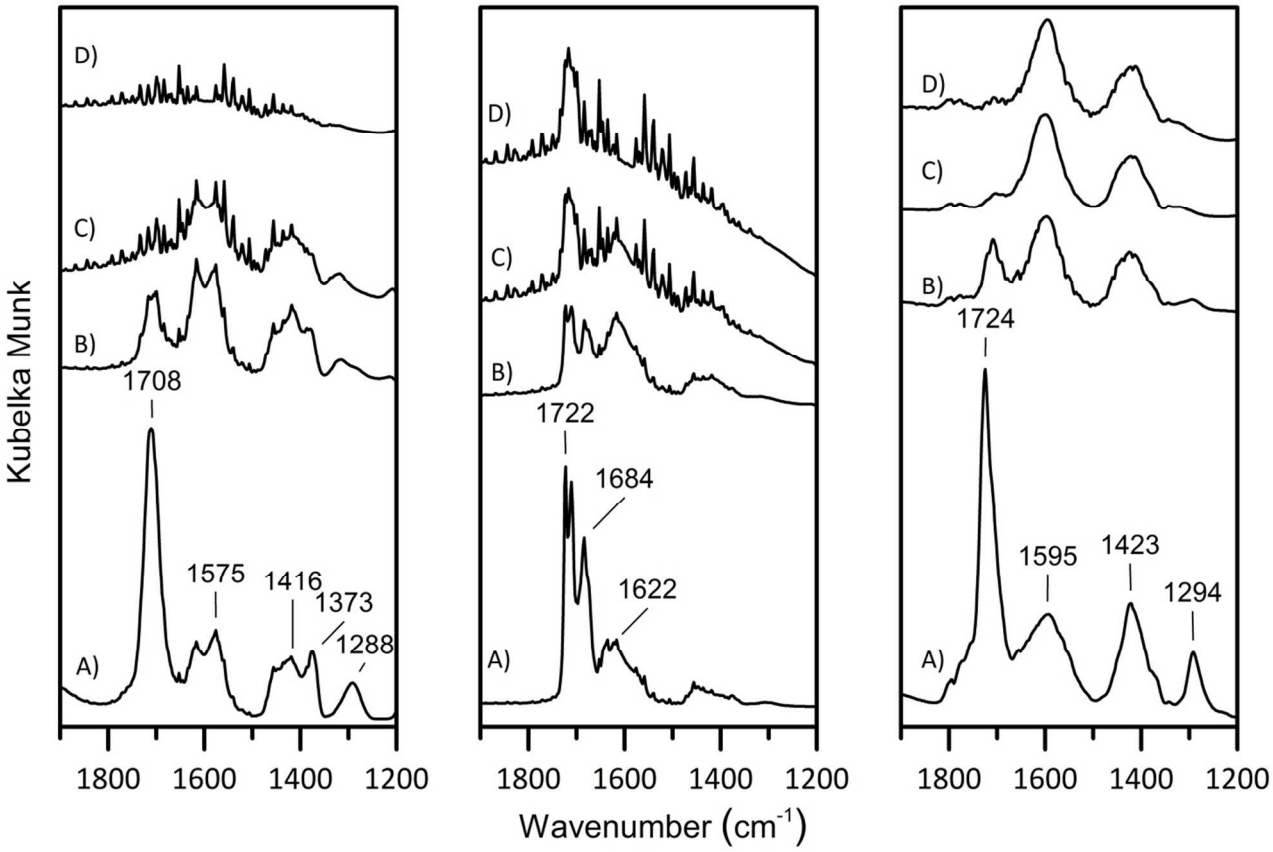

Figure 7. DRIFTS spectra of the C=O stretching region for adsorbed acetaldehyde (left), crotonaldehyde (center), acetic acid (right) on TiO_2 after purging at A) 303 K, B) 373 K, C) 473 K and D) 573 K.

For acetaldehyde adsorption on TiO_2, the peak at 1708 cm^{-1} can be assigned to the C=O stretching mode of acetaldehyde while the peak at 1373 cm^{-1} can be assigned to the $\delta(CH_3)$ mode of acetaldehyde, which are in good agreement with features observed by Rekoske and Barteau.[36] Neither of those features were observed above 373 K indicating acetaldehyde is weakly held on TiO_2. The features at 1575, 1416 and 1288 cm^{-1} are very similar in shape and thermal response as the features observed during acetic acid adsorption and therefore are likely attributed to a

surface acetate species. The acetate species is probably formed from a Cannizzaro reaction that has been shown to take place on basic surfaces such as MgO.[37] The fact that the peak at 1708 cm^{-1} is gone by 473 K implies that intact acetaldehyde is not strongly held to the TiO_2 surface. Acetate, on the other hand, appears to be a more strongly bound species which remains on the surface to at least 573 K. Adsorbed crotonaldehyde has a feature at 1684 cm^{-1} which can be assigned to the C=O stretching mode and is in good agreement with the work of Rekoske and Barteau.[36] The features at 1722 and 1622 cm^{-1} are currently unassigned but may be due to poly-condensation products. The feature observed at 1724 cm^{-1} in the spectrum of adsorbed acetic acid is likely due to the C=O stretching of the acid group. Since this peak disappears by 373 K, the adsorbed acid is very weakly held on TiO_2. The broad peaks at 1595 and 1423 cm^{-1} are present up to 573 K and are likely due to a strongly adsorbed acetate species.

The effect of pre-adsorbed ethanol on the adsorption of acetaldehyde on TiO_2 is shown in Figure 8. The presence of adsorbed ethanol is clear due to the features in the C-H stretching region of the IR spectrum. Adsorbed ethanol does not appear to affect the features of adsorbed acetaldehyde. Thus, based on the large observed inhibition of acetaldehyde condensation by ethanol during catalysis, we suspect that ethanol simply competes for active sites on the surface.

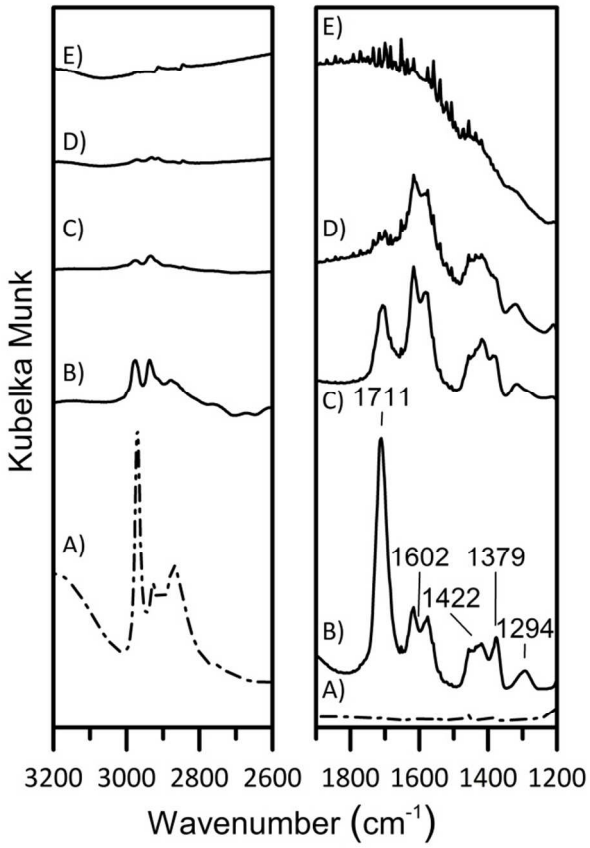

Figure 8. DRIFTS spectra of adsorbed acetaldehyde with preadsorbed ethanol on TiO_2. A) adsorbed ethanol after purging at 303 K, adsorbed acetaldehyde and ethanol after purging at B) 303 K, C) 373 K, D) 473 K and E) 573 K.

Figure 9 shows the C=O stretching region of the probe molecules adsorbed on HAP. Adsorbed acetaldehyde shows two features at 1707 and 1572 cm^{-1}. The peak at 1707 cm^{-1} can be assigned to the C=O stretching mode of acetaldehyde. The 1707 cm^{-1} feature completely disappeared by 473 K while the 1572 cm^{-1} feature was still observed at 673 K. Adsorbed crotonaldehyde has two major features at 1674 and 1601 cm^{-1}. As with adsorbed acetaldehyde, the 1674 cm^{-1} peak disappeared by 473 K while the feature at 1601 cm^{-1} was present up to 573 K. Adsorption of

acetic acid resulted in 4 major peaks: 1707, 1661, 1562, and 1298 cm^{-1}. The features at 1707 and 1298 cm^{-1} were no longer observed at 473 K and the intensity of the 1661 and 1562 cm^{-1} peaks decreased as the temperature was increased.

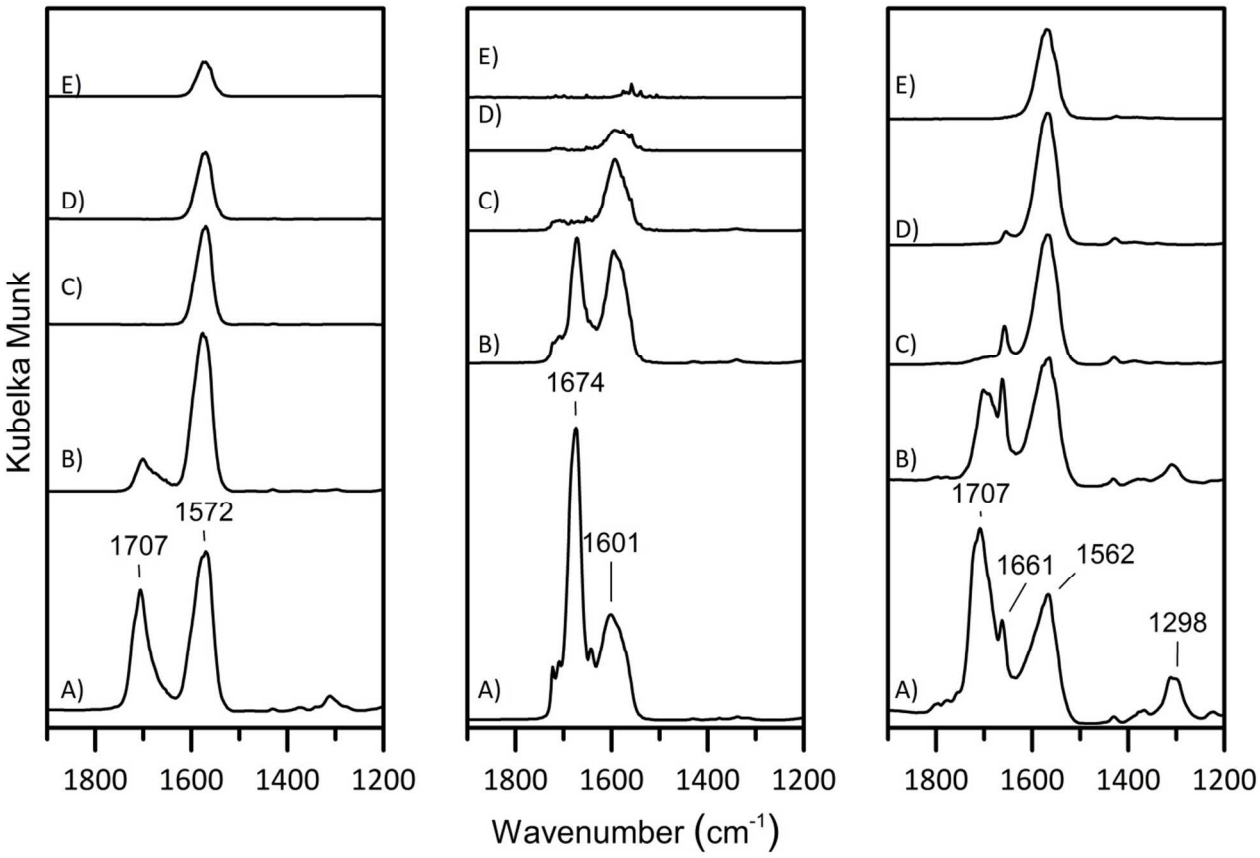

Figure 9. DRIFTS spectra of the C=O stretching region for adsorbed acetaldehyde (left), crotonaldehyde (center), acetic acid (right) on HAP after purging at A) 303 K, B) 373 K, C) 473 K, D) 573 K and E) 673 K.

The 1707 cm^{-1} feature in the spectrum of adsorbed acetaldehyde on HAP that is assigned to the C=O stretching mode is in good agreement with work by Rekoske and Barteau with acetaldehyde adsorbed on rutile titania (1703 cm^{-1}).[36] This peak is approximately 30 cm^{-1} red

shifted from gas phase acetaldehyde because of interactions with the surface. The feature at 1572 cm^{-1} is likely an indication of adsorbed acetate. Strongly bound acetate species on HAP have been reported previously by Tanaka et al.[38] in which they show acetate features at 1574 and 1545 cm^{-1} remain on HAP up to temperatures of 723 K. The spectra in Figure 9 reveal the presence of acetate after acetaldehyde adsorption at room temperature, indicating a high reactivity of acetaldehyde on HAP even at low temperature. The high reactivity of acetaldehyde on HAP may explain the measured high heat of adsorption during acetaldehyde adsorption microcalorimetry (Figure 5).

The spectrum of adsorbed crotonaldehyde on HAP revealed similar features as that for adsorbed acetaldehyde (Figure 9). A peak at 1674 cm^{-1} is observed at 373 K while the feature at 1601 cm^{-1} is present up to 573 K. The peak at 1674 cm^{-1} is attributed to the C=O stretching mode of crotonaldehyde, which is 40 cm^{-1} red shifted from gas phase crotonaldehyde. It is not clear what the feature at 1601 cm^{-1} results from and may be either a C_4 carboxylate or the C=C stretching mode of crotonaldehyde.

Acetic acid adsorption on HAP initially resulted in 4 major features at 1707, 1661, 1562, and 1298 cm^{-1}. The band at 1707 cm^{-1} can be assigned to the C=O stretching mode of the acid while the band at 1562 cm^{-1} is due to the C=O stretch of an acetate species. At low temperature, both the acid and the acetate species are present, but at high temperature only the peak associated with acetate is observed. Our results are in good agreement with Tanaka et al.[38] who claimed that acetic acid adsorbs as a weakly-bound acid species as well as a strongly-bound acetate species.

Figure 10 shows the effect of pre-adsorbed ethanol on acetaldehyde adsorption on HAP. Pre-adsorbed ethanol was confirmed on the surface of HAP by the presence of features in the C-H stretching region. After adsorbing acetaldehyde, the intensity of the C-H stretching peaks

decreased while multiple peaks appeared in the C=O stretching region. There are features at 1703, 1666, 1641 and 1568 cm^{-1}. The peaks at 1703, 1666 and 1641 cm^{-1} decrease as the temperature is increased while the peak at 1568 cm^{-1} increased in intensity after heating to 473 K before slightly decreasing at higher temperature.

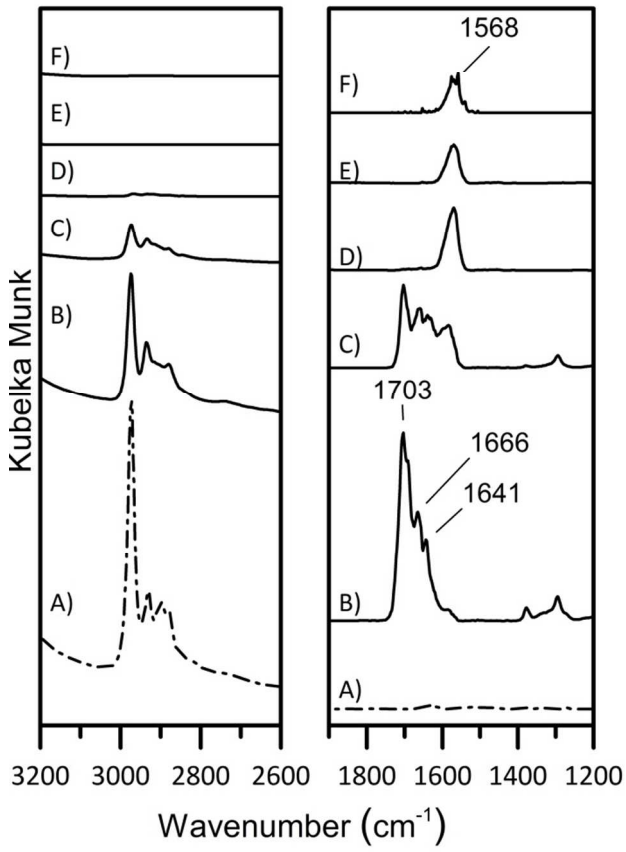

Figure 10. DRIFTS spectra of adsorbed acetaldehyde with preadsorbed ethanol on HAP. A) adsorbed ethanol after purging at 303 K, adsorbed acetaldehyde and ethanol after purging at B) 303 K, C) 373 K, D) 473 K, E) 573 K and F) 673 K.

Preadsorbed ethanol clearly had an influence on acetaldehyde adsorption on HAP. The main difference between adsorption of acetaldehyde with and without preadsorbed ethanol is that

ethanol prevents the formation of acetate at low temperature. As the temperature is increased, weakly bound ethanol desorbs from HAP and allows adsorbed acetaldehyde to form strongly bound acetate species.

Figure 11 shows the carbonyl stretching region of acetaldehyde, crotonaldehyde, and acetic acid adsorbed on MgO. There are four major features for acetaldehyde adsorbed on MgO, a peak at 1719 cm^{-1} observed up to 373 K, two broad peaks at 1584 and 1442 cm^{-1} that are present even at 673 K, and a feature at 1326 cm^{-1} observed up to 573 K. The spectra of adsorbed crotonaldehyde reveal similar features to those of adsorbed acetaldehyde, a peak at 1719 cm^{-1} present up to 373 K, and two broad peaks at 1574 and 1444 cm^{-1} that are present up to 673 K. The spectra of adsorbed acetic acid have four features, a peak at 1709 cm^{-1} that is present at 303 K, but not at higher temperatures, a peak at 1341 cm^{-1} present up to 573 K and two broad peaks at 1599 and 1425 cm^{-1} that are present up to 673 K with maximum intensity at 573 K.

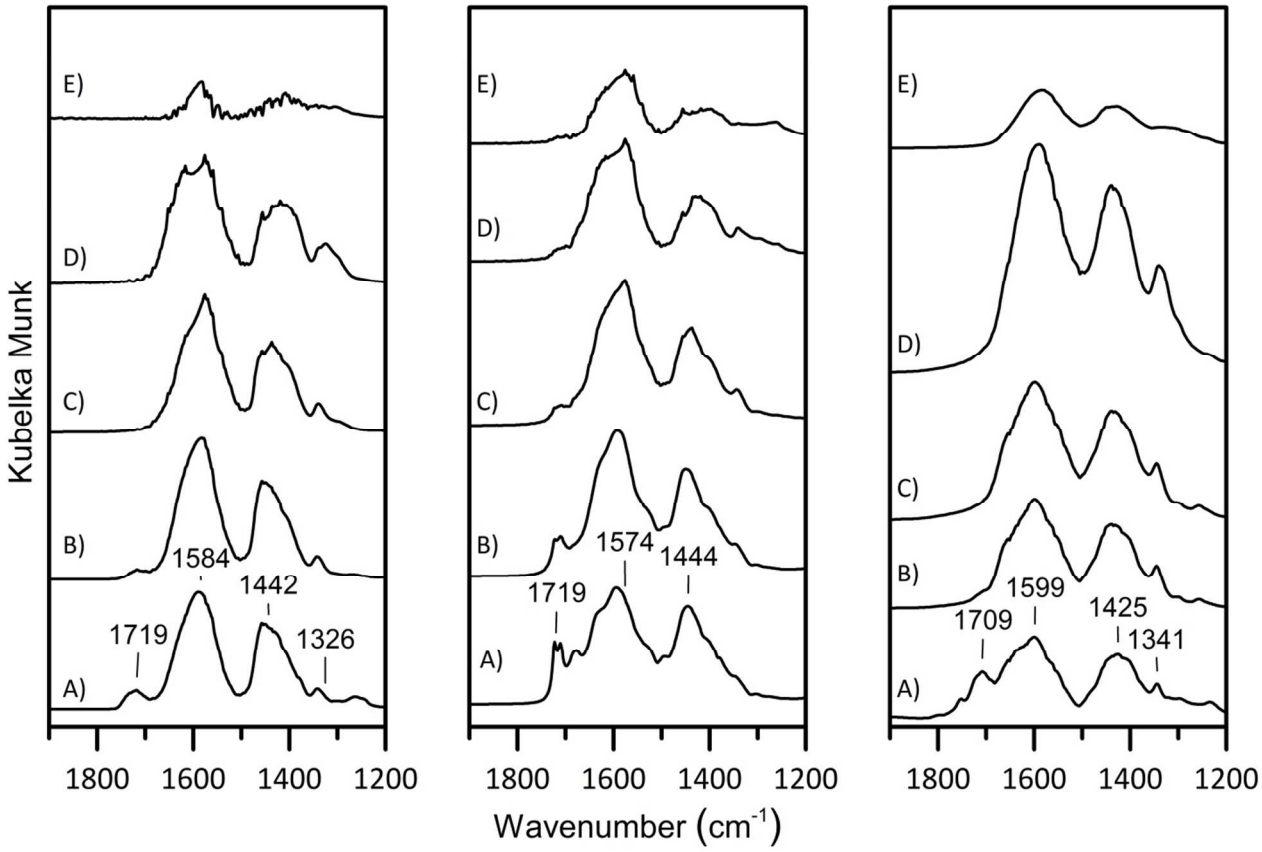

Figure 11. DRIFTS spectra of the C=O stretching region for adsorbed acetaldehyde (left), crotonaldehyde (center), acetic acid (right) on MgO after purging at A) 303 K, B) 373 K, C) 473 K, D) 573 K and E) 673 K.

The peak at 1719 cm^{-1} can be assigned to the C=O stretching of adsorbed acetaldehyde on MgO, which disappears by 473 K, indicating it is weakly adsorbed. The peaks at 1584, 1442 and 1326 cm^{-1} are quite similar to the main features observed with acetic acid adsorption on MgO and are attributed to surface acetate. The fact that these peaks are present up to 673 K shows that acetate was very strongly bound to the surface. The peak at 1719 cm^{-1} in the spectra of adsorbed crotonaldehyde is likely due to the C=O stretching of crotonaldehyde and since it disappears by

473 K, indicating crotonaldehyde is relatively weakly adsorbed compared to acetaldehyde. The peaks at 1574 and 1444 cm^{-1} are attributed to either a surface carboxylate or to poly condensation products of crotonaldehyde. The minor peak at 1709 cm^{-1} in the spectra of acetic acid is likely caused by the C=O stretching of the acid, whereas the majority of the peaks are associated with acetate species.

The effect of preadsorbed ethanol on MgO prior to acetaldehyde adsorption is presented in Figure 12. The similarity between Figure 11 and 12 indicates preadsorption of ethanol on MgO had very little effect on IR features present after acetaldehyde adsorption.

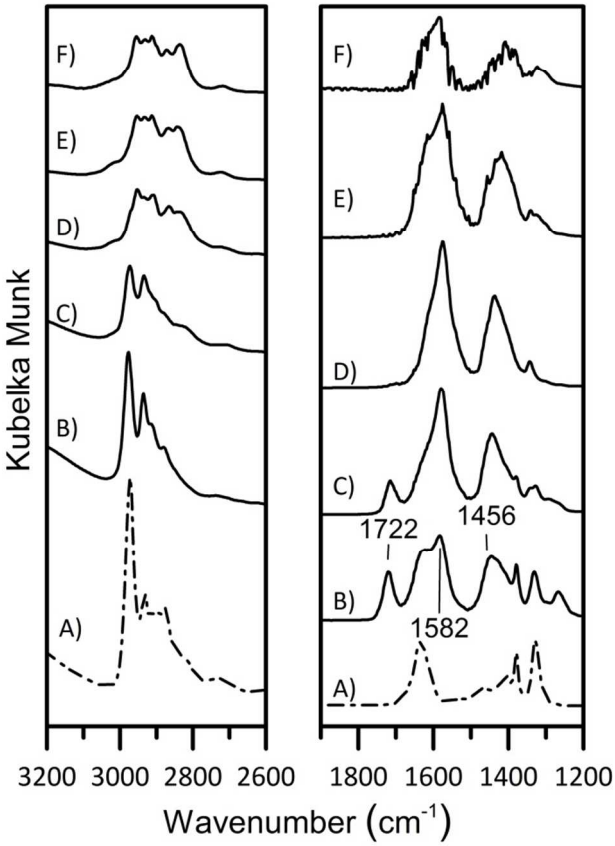

Figure 12. DRIFTS spectra of adsorbed acetaldehyde with preadsorbed ethanol on MgO. A) adsorbed ethanol at 303 K, adsorbed acetaldehyde and ethanol after purging at B) 303 K, C) 373 K, D) 473 K, E) 573 K and F) 673 K.

4. Conclusions

Aldol condensation occurs readily over TiO_2, HAP and MgO, producing only crotonaldehyde at low conversion. However, severe deactivation was observed at high acetaldehyde partial pressures. Initial rate measurements were therefore used to examine the influence of acetaldehyde pressure and reaction temperature on the kinetics and to rank the activity of the catalysts. Results revealed an activity ranking per surface area of TiO_2>HAP>>MgO. Aldol condensation using fully deuterated acetaldehyde showed no kinetic isotope effect indicating that C-H bond activation is not kinetically relevant. A plausible mechanism of aldol condensation over these materials consists of kinetically relevant reactant adsorption and product desorption steps. At the conditions used here, the presence of ethanol had no effect on the rate of aldol condensation over HAP or MgO, but inhibited the rate of aldol condensation over TiO_2. The performance of the materials in aldol condensation can be related to the relative affinity of the surface for aldehydes, and other intermediate species with TiO_2 having the lowest affinity (greatest reaction rate) and MgO having the greatest affinity (lowest reaction rate). The weak affinity of TiO_2 for the reacting species accounts for the inhibiting effect of ethanol on the aldol condensation rate because of the competitive adsorption.

Supporting Information

Supporting Information Available: The XRD patterns, the rate of reaction versus time on stream, and a derivation of the kinetic model used can be found in the Supporting Information. This material is available free of charge via the Internet at http://pubs.acs.org

Acknowledgements

This work was funded by the U.S. Department of Energy. Grant No. DE-FG02-95ER14549

References

(1) Di Cosimo, J. I.; Díez, V. K.; Xu, M.; Iglesia, E.; Apesteguía, C. R. *J. Catal.* **1998**, *178*, 499–510.

(2) Birky, T. W.; Kozlowski, J. T.; Davis, R. J. *J. Catal.* **2013**, *298*, 130–137.

(3) Ndou, A. S.; Plint, N.; Coville, N. J. *Appl. Catal. A Gen.* **2003**, *251*, 337–345.

(4) Tsuchida, T.; Kubo, J.; Yoshioka, T.; Sakuma, S.; Takeguchi, T.; Ueda, W. *J. Catal.* **2008**, *259*, 183–189.

(5) Hanspal, S.; Young, Z. D.; Shou, H.; Davis, R. J. *ACS Catal.* **2015**, 1737–1746.

(6) Ordóñez, S.; Díaz, E.; León, M.; Faba, L. *Catal. Today* **2010**, *167*, 71–76.

(7) Tsuchida, T.; Sakuma, S.; Takeguchi, T.; Ueda, W. *Ind. Eng. Chem. Res.* **2006**, *45*, 8634–8642.

(8) Ogo, S.; Onda, A.; Iwasa, Y.; Hara, K.; Fukuoka, A.; Yanagisawa, K. *J. Catal.* **2012**, *296*, 24–30.

(9) Tsuchida, T.; Kubo, J.; Yoshioka, T.; Sakuma, S.; Takeguchi, T.; Ueda, W. *J. Japan Pet. Inst.* **2009**, *52*, 51–59.

(10) Ogo, S.; Onda, A.; Yanagisawa, K. *Appl. Catal. A Gen.* **2011**, *402*, 188–195.

(11) Kozlowski, J. T.; Davis, R. J. *ACS Catal.* **2013**, *3*, 1588–1600.

(12) Kibby, C. L.; Hall, W. K. *J. Catal.* **1973**, *31*, 65–73.

(13) Ho, C. R.; Shylesh, S.; Bell, A. T. *ACS Catal.* **2016**, *6*, 939–948.

(14) Scalbert, J.; Thibault-Starzyk, F.; Jacquot, R.; Morvan, D.; Meunier, F. *J. Catal.* **2014**, *311*, 28–32.

(15) Chieregato, A.; Velasquez Ochoa, J.; Bandinelli, C.; Fornasari, G.; Cavani, F.; Mella, M. *ChemSusChem* **2015**, *8*, 377–388.

(16) Biaglow, A. *J. Catal.* **1995**, *151*, 373–384.

(17) Dumitriu, E.; Hulea, V.; Chelaru, C.; Catrinescu, C.; Tichit, D.; Durand, R. *Appl. Catal. A Gen.* **1999**, *178*, 145–157.

(18) Tichit, D.; Lutic, D.; Coq, B.; Durand, R.; Teissier, R. *J. Catal.* **2003**, *219*, 167–175.

(19) Abelló, S.; Medina, F.; Tichit, D.; Pérez-Ramírez, J.; Groen, J. C.; Sueiras, J. E.; Salagre, P.; Cesteros, Y. *Chem. Eur. J.* **2005**, *11*, 728–739.

(20) Sharma, S. K.; Parikh, P. a.; Jasra, R. V. *J. Mol. Catal. A Chem.* **2007**, *278*, 135–144.

(21) Reichle, W. *J. Catal.* **1980**, *63*, 295–306.

(22) Shen, W.; Tompsett, G. a.; Xing, R.; Curtis Conner, W.; Huber, G. W. *J. Catal.* **2012**, *286*, 248–259.

(23) Raskó, J.; Kiss, J. *Appl. Catal. A Gen.* **2005**, *287*, 252–260.

(24) Ordomsky, V. V.; Sushkevich, V. L.; Ivanova, I. I. *J. Mol. Catal. A Chem.* **2010**, *333*, 85–93.

(25) Di Cosimo, J. I.; Diez, V.; Apesteguia, C. *Appl. Catal. A Gen.* **1996**, *137*, 149–166.

(26) Ai, M. *Bull. Chem. Soc. Jpn.* **1991**, *64*, 1342–1345.

(27) Rekoske, J. E.; Barteau, M. a. *Ind. Eng. Chem. Res.* **2011**, *50*, 41–51.

(28) Luo, S.; Falconer, J. L. *J. Catal.* **1999**, *185*, 393–407.

(29) Idriss, H.; Diagne, C.; Hindermann, J. P.; Kiennemann, A.; Barteau, M. A. *J. Catal.* **1995**, *155*, 219–237.

(30) Rodrigues, E. G.; Keller, T. C.; Mitchell, S.; Pérez-Ramírez, J. *Green Chem.* **2014**, *16*, 4870–4874.

(31) Bordawekar, S. V.; Doskocil, E. J.; Davis, R. J. *Langmuir* **1998**, *14*, 1734–1738.

(32) Bordawekar, S. V.; Davis, R. J. *J. Catal.* **2000**, *189*, 79–90.

(33) Kozlowski, J. T.; Aronson, M. T.; Davis, R. J. *Appl. Catal. B Environ.* **2010**, *96*, 508–515.

(34) Doskocil, E. J.; Bordawekar, S. V.; Davis, R. J. *J. Catal.* **1997**, *169*, 327–337.

(35) Forzatti, P.; Lietti, L. *Catal. Today* **1999**, *52*, 165–181.

(36) Rekoske, J. E.; Barteau, M. A. *Langmuir* **1999**, *15*, 2061–2070.

(37) Peng, X.; Barteau, M. *Langmuir* **1989**, *5*, 1051–1056.

(38) Tanaka, H.; Watanabe, T.; Masatoshi Chikazawa, A. *J. Chem. Soc. Faraday Trans.* **1997**, *93*, 4377–4381.

Graphical Abstract